buildings

MDPI

Article

Seismic Performance Assessment of Composite Frame–High-Strength Steel Plate Wall Core Tube Resilient Structural System

Lei Zhang *, Cuikun Wang, Caihua Chen * and Mingzhe Cui

China Academy of Building Research, Beijing 100013, China; wangcuikun@cabrtech.com (C.W.); cuimingzhe@cabrtech.com (M.C.)
* Correspondence: zhanglei1@cabrtech.com (L.Z.); chencaihua@cabrtech.com (C.C.)

Abstract: Against the backdrop of China's continuous promotion of green and low-carbon transformation and the development of construction industrialization, high-strength composite structural systems have significant development prospects. However, their research and application in the field of construction are insufficient. In response to this issue, the study proposes a new high-performance structural system, namely the composite frame–high-strength steel plate wall core tube resilient structural system, which includes a core tube composed of double steel plate concrete composite shear walls and replaceable energy dissipation coupling beams, as well as composite frames. The highest strength grades of the steel plate and concrete used in the composite walls of the core tube are Q550 and C100, respectively. Using a 200 m building as an example, this study designs and establishes models for this high-performance structure and a conventional reinforced concrete frame–core tube structure. Subsequently, the dynamic elastoplastic time history analysis and seismic resilience assessment of structures are conducted under design basis earthquakes (DBEs), maximum considered earthquakes (MCEs), and extremely rare earthquakes (EREs). Research has shown that, compared to conventional structures, the thickness of shear walls of new high-performance structures can be effectively reduced, which helps decrease the self-weight of the structure and improve the available space in buildings. Additionally, high-performance structures exhibit a better performance in controlling the story drift ratio, lower plastic damage and overall stiffness degradation of the structure, and better seismic performance. The seismic resilience of the high-performance structure has been significantly enhanced, especially in terms of minimizing casualties, thereby better ensuring the safety of people's lives and property.

Keywords: high-performance structural system; high-strength steel; ultra-high-strength concrete; double steel plate concrete composite shear wall; seismic resilience assessment

Citation: Zhang, L.; Wang, C.; Chen, C.; Cui, M. Seismic Performance Assessment of Composite Frame–High-Strength Steel Plate Wall Core Tube Resilient Structural System. *Buildings* **2024**, *14*, 301. https://doi.org/10.3390/buildings14010301

Academic Editors: Mu-Xuan Tao and Li-Yan Xu

Received: 8 December 2023
Revised: 17 January 2024
Accepted: 20 January 2024
Published: 22 January 2024

1. Introduction

Since the 1990s, performance-based seismic design [1–4] has gradually become the main development direction of seismic design. Due to the inherent uncertainty and complexity of earthquakes, buildings often encounter earthquakes that exceed their capacity for fortification, rendering repair efforts challenging and severely disrupting people's daily lives. Consequently, the seismic performance objectives progressively transition from prioritizing life safety to reinstating the building's functional capacity. In January 2009, at the NEES/E-Defense United States Japan Earthquake Engineering Phase II Cooperation Research Plan Conference, scholars from the United States and Japan proposed for the first time that "resilient cities" should be the direction of earthquake engineering cooperation [5]. The development of "resilient cities" has emerged as a crucial aspect of urban planning during China's 14th Five-Year Plan period. Enhancing the seismic resilience of buildings has become a pivotal research focus within the field of seismic engineering.

Simultaneously, in the context of China's ongoing promotion of green low-carbon transformation and the advancement of building industrialization, it is imperative to develop a high-performance steel plate concrete composite structure system that integrates high-strength steel and high-strength, high-performance concrete. This will enable the achievement of a harmonious combination of enhanced load-bearing capacity, disaster resistance, lightweight characteristics, and ease of construction through the utilization of prefabricated assembly components [6–10], thereby facilitating its widespread application in large-scale industrial and civil buildings.

The shear wall, extensively utilized in tall buildings, assumes a pivotal role in enhancing the seismic resistance of structures. The conventional reinforced concrete shear wall exhibits excessive weight and susceptibility to cracking, while the lower portion of tall buildings' reinforced concrete walls is prone to damage during intense seismic events [11]. Compared to traditional reinforced concrete shear walls, steel plate concrete shear walls can significantly enhance the load-bearing capacity, energy dissipation capacity, and ductility of structural members. The double-sided steel plate shear wall eliminates the need for internal steel reinforcement, thereby reducing the construction complexity. Additionally, by positioning the steel plates on the outermost layer, their mechanical performance can be maximized [12]. Currently, numerous scholars have conducted extensive research on the mechanical properties and seismic performance of conventional strength steel plate concrete composite shear walls, which have been verified to possess excellent ductility and load-bearing capacity [13–17]. The design and construction requirements for conventional strength steel–concrete composite shear walls are well established in national and industry design codes [18,19]. Moreover, the steel plate concrete composite shear wall has been implemented in super tall buildings [20–22].

Currently, significant advancements have been made in the research and application of high-strength steel and high-performance concrete. Q550 grade high-strength steel and C120 grade high-strength concrete have been applied in various fields including bridges. However, there is relatively little research and application of high-strength materials in the construction field. In current building specifications, the concrete strength of steel plate–concrete composite structures can reach up to C80, while the steel plate strength can go as high as Q460. However, this somewhat restricts the application of high-strength materials in constructing super tall buildings. The latest research on high strength concrete structures indicates that the utilization of C100 high strength concrete shear walls, combined with a well-designed system, effectively ensures the overall seismic safety of the structure [23]. The research findings demonstrate that the incorporation of steel plates in steel plate–concrete composite shear walls effectively mitigates the inherent brittleness associated with high-strength concrete. Currently, the research and application have been limited to steel plates below Q460 and concrete below C80 [24–28], necessitating further investigation into higher strength combinations.

Currently, the construction of super tall buildings exceeding 250 m is subject to restrictions in China; therefore, this study focuses on 200 m tall buildings as a representative example. The predominant structural system for super tall buildings within this height range is the frame–core tube configuration. Therefore, to enhance the structural seismic resilience, mitigate carbon emissions from the building, and optimize the construction economics, this paper proposes a composite frame high-strength steel plate wall core tube resilient structural system suitable for super tall buildings. The steel utilized in this system exhibits a maximum strength of Q550, while the concrete possesses a maximum strength of C100. This paper provides a detailed introduction to the main components of the new high-performance structural system, and presents the performance objectives of this system and its key components under service-level earthquakes (SLEs), design basis earthquakes (DBEs), and maximum considered earthquake (MCEs). Simultaneously, to validate the seismic performance of the proposed high-performance structural system, the paper employs PKPK 2023 building structure design software to conceive and establish two 200 m-level frame core tube structures: a conventional reinforced concrete frame core tube structure

and a new high-performance frame–core tube structure. Subsequently, elastic analysis and reinforcement design are conducted. Based on the commonly used finite element analysis software SAUSAGE 2023 (abbreviated as SSG hereafter) in China, an elastoplastic analysis model was established for the two aforementioned models. The dynamic elastoplastic time history analysis of the structure was conducted to evaluate its seismic performance under DBEs, MCEs, and extremely rare earthquakes (EREs). Furthermore, a comprehensive summary of the seismic response of the high-performance structural system under MCEs was provided. Finally, utilizing the seismic resilience assessment program developed by the research group [29] in accordance with the Standard for seismic resilience assessment of buildings (GB/T 38591-2020) [30] (hereinafter referred to as the Resilience Standard), coupled with supplementary survey and statistical data on the vulnerability parameter values of composite components, a comprehensive seismic resilience assessment is conducted for each model.

2. Overview of High-Performance Structural Systems

2.1. System Composition

The proposed structural system in this paper primarily consists of a composite frame and a high-strength steel plate concrete core tube (Figure 1). Among them, the high-strength steel plate–concrete core tube is composed of high-strength steel plate–ultra-high-strength concrete shear walls and replaceable energy dissipation coupling beams (Figure 2). The proposed system is designed to accomplish the following objectives:

(1) Energy consumption during MCEs is primarily concentrated in the frame beam and the replaceable energy dissipation coupling beam. The frame column and shear wall remain undamaged, ensuring rapid structural repair post-earthquake and enhancing the seismic resilience of the structure.
(2) The high-performance structural system, composed of high-strength steel and high-strength concrete, effectively optimizes the material utilization and achieves the objective of energy conservation and emission reduction in buildings.
(3) Compared to the conventional frame–core tube structure, the high-performance structural system offers potential cost savings and enhances the economic efficiency of structural construction.

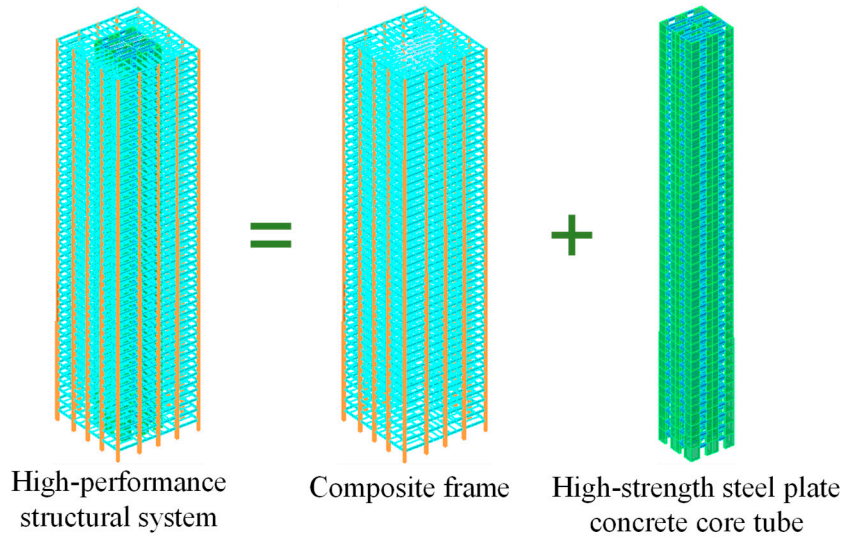

Figure 1. Composite frame—high-strength steel plate wall core tube resilient structural system.

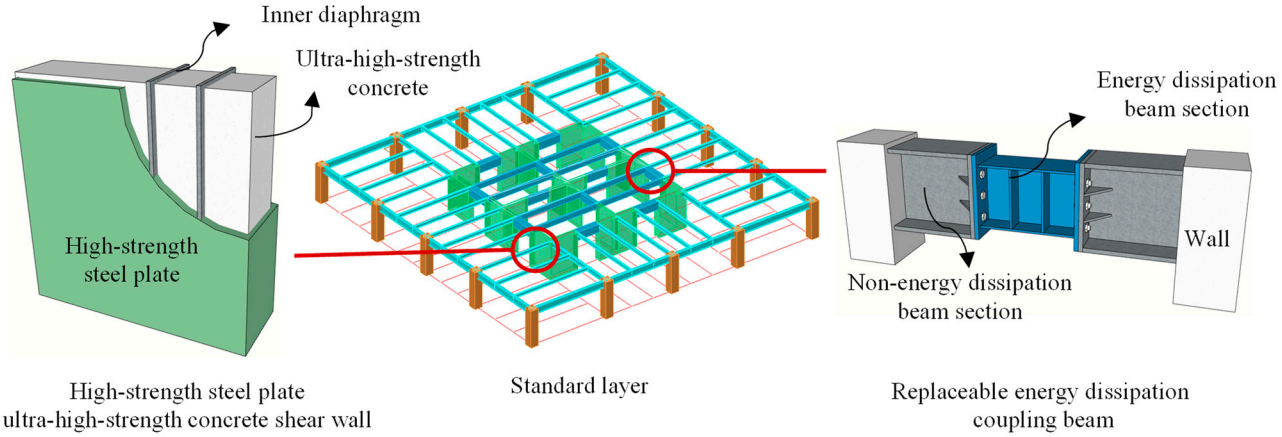

Figure 2. Diagram of the high-strength steel plate ultra-high-strength concrete shear wall and the replaceable energy dissipation coupling beam.

2.2. Performance Objectives

The seismic performance objectives for various structural components are presented in Table 1, and the overall performance objectives are in accordance with the seismic performance objective C defined in the Technical Specification for Concrete Structures of Tall Buildings (JGJ 3-2010) [31] (hereinafter referred to as the Tall Buildings Design Code).

Table 1. The seismic performance objectives for various structural components.

Type	Classification	SLE	DBE	MCE
Overall structure	Story drift ratio	Concrete structure: 1/620 Steel structure: 1/250	-	Concrete structure: 1/100 Steel structure: 1/50
	Residual story drift ratio	0	-	0.50%
Key components	Core tube and frame columns of bottom stiffened area	Normal section elasticity Inclined section elasticity	Normal section elasticity Inclined section elasticity	Normal section unyielding under pressure Inclined section elasticity
Common components	Core tube and frame columns of other stories	Normal section elasticity Inclined section elasticity	Normal section unyielding Inclined section elasticity	Minimum shear section (moderate damage to some components)
Energy dissipation components	Frame beams	Normal section elasticity Inclined section elasticity	Inclined section elasticity	Plastic energy dissipation
	Coupling beams	Normal section elasticity Inclined section elasticity	Plastic energy dissipation	Plastic energy dissipation

3. Analysis Model

3.1. Basic Design Information

The research object is a frame–core tube structure, with a fortification intensity of 7 (design basic ground motion acceleration of structures under DBEs is 0.15 g, g = 9.8 m/s^2), site class II and design earthquake classification I specified in the Code for Seismic Design of Buildings (GB 50011-2010) [32] (hereinafter referred to as the Seismic Design Code). The height of the structure is 198.4 m, with a total of 46 stories and an aspect ratio of 4.4. The plane size of the outer frame is 45 m × 45 m, with a core tube plane size of 21 m × 21 m.

In order to investigate the seismic performance of the structure, two models have been designed and established based on PKPM and with Table 1 as the seismic performance objective. The first model is referred to as the conventional frame core tube design model (referred to as the conventional model, denoted by BM-7.5-C-P), while the second model is known

as the high-performance frame core tube design model (referred to as the high-performance model, denoted as HP-7.5-C-P). The layout of these models is illustrated in Figure 3.

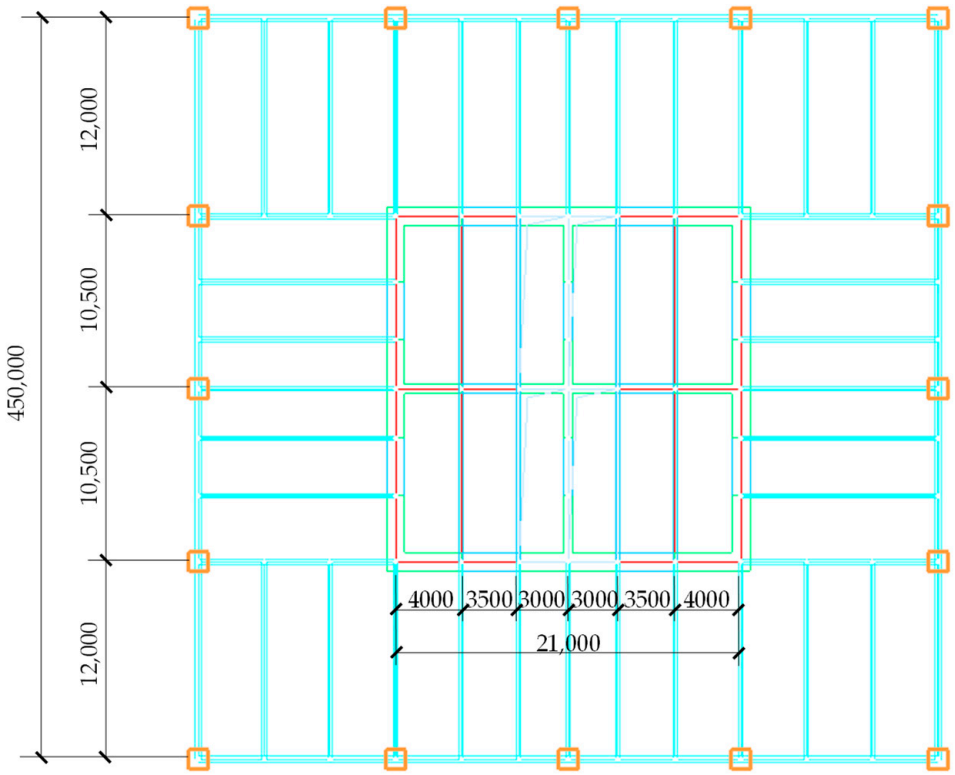

Figure 3. The structural layout.

The outer frame columns of both models are both concrete-filled square steel tubular columns (CFSSTCs), and the outer frame beams and the connecting beams between the outer frame and the core tube are all H-shaped steel beams. The connection between the outer frame beam and the outer frame column is rigid, while the connecting beam is hinged at both ends. The primary distinction between the two models lies in their core tubes. Specifically, the core tube of BM-7.5-C-P consists of the reinforced concrete shear walls and reinforced concrete coupling beams, whereas the core tube of HP-7.5-C-P is composed of a high-strength steel plate–ultra-high-strength concrete shear walls and replaceable energy dissipation coupling beams. The material consumption of the two models is presented in Table 2, while the high-performance model demonstrates a total reduction in structural weight of 17% compared to the conventional model. The cross-sectional dimensions and material details of the main structural components for both models are provided in Tables 3 and 4, respectively.

Table 2. The main material consumption of the two models.

Material	Unit	Model	
		BM-7.5-C-P	HP-7.5-C-P
Concrete	m^3	25,349	19,988 (−21%)
	t	65,908	51,968 (−21%)
Steel	t	7271	10,048 (+38%)
Rebar	t	2829	983 (−65%)
Total	t	76,008	62,999 (−17%)

Table 3. The cross-sectional dimensions and material details of the main structural components of BM-7.5-C-P.

Story	Core Tube							Outer Frame			
	t_{EW} (mm)	A_{ES} (mm^2)	t_{IW} (mm)	A_{IS} (mm^2)	H_{CB} (mm)	Concrete Grade	Steel Grade	Section of Column (mm)	Section of Beam (mm)	Concrete Grade	Steel Grade
L1~L2	1000	1,933,000	450	92,000	1200	C70	Q355	1300 × 1300 × 30	H1000 × 400 × 16 × 25	C60	Q355
L3~L6	900	1,757,500	450	85,000	1200	C70	Q355	1200 × 1200 × 25	H1000 × 400 × 16 × 25	C60	Q355
L7~L11	800		400		1200	C70		1200 × 1200 × 25	H1000 × 400 × 16 × 25	C60	Q355
L12~L16	700		400		1200	C60		1100 × 1100 × 25	H1000 × 400 × 16 × 25	C60	Q355
L17~L21	700		350		1200	C60		1000 × 1000 × 22	H1000 × 400 × 16 × 25	C60	Q355
L22~L26	700		350		1200	C50		900 × 900 × 20	H1000 × 400 × 16 × 25	C50	Q355
L27~L31	600		300		1200	C50		800 × 800 × 18	H1000 × 400 × 16 × 25	C50	Q355
L32~L36	500		300		1200	C50		800 × 800 × 18	H1000 × 400 × 16 × 25	C50	Q355
L37~L41	500		250		1200	C40		800 × 800 × 18	H1000 × 400 × 16 × 25	C40	Q355
L42~L46	400		250		1200	C40		800 × 800 × 18	H1000 × 400 × 16 × 25	C40	Q355

Note: Thickness of exterior wall t_{EW}, total section area of steel in exterior wall A_{ES}, thickness of interior wall t_{IW}, total section area of steel in interior wall A_{IS}, and height of coupling beam H_{CB}.

Table 4. The cross-sectional dimensions and material details of the main structural components of HP-7.5-C-P.

Story	Core Tube											
	Exterior Wall				Coupling Beam of Exterior Wall		Interior Wall				Coupling Beam of Interior Wall	
	t_{EW} (mm)	t_{SE} (mm)	Concrete Grade	Steel Grade	Non-Energy Dissipation Beam Section (mm)	Energy Dissipation Beam Section (mm)	t_{IW} (mm)	t_{SI} (mm)	Concrete Grade	Steel Grade	Non-Energy Dissipation Beam Section (mm)	Energy Dissipation Beam Section (mm)
L1~L2	700	16	C100	Q550	H1200 × 450 × 25 × 35	H1000 × 420 × 25 × 25	250	10	C100	Q355	H1000 × 250 × 20 × 35	H750 × 250 × 12 × 25
L3~L6	600	14	C100	Q550	H1200 × 450 × 25 × 35	H1000 × 420 × 25 × 25	250	10	C100	Q355	H1000 × 250 × 20 × 35	H750 × 250 × 12 × 25
L7~L11	500	12	C90	Q550	H1200 × 450 × 25 × 35	H1000 × 400 × 25 × 25	250	10	C90	Q355	H1000 × 250 × 20 × 35	H750 × 250 × 12 × 25
L12~L16	400	10	C80	Q460	H1200 × 400 × 25 × 30	H1000 × 400 × 20 × 20	250	10	C80	Q355	H800 × 250 × 16 × 30	H600 × 250 × 12 × 20
L17~L21	350	10	C70	Q420	H1000 × 300 × 20 × 30	H800 × 300 × 15 × 20	250	10	C70	Q355	H800 × 250 × 16 × 30	H600 × 250 × 12 × 20
L22~L26	300	10	C60	Q355	H1000 × 300 × 20 × 30	H800 × 300 × 15 × 20	250	10	C60	Q355	H800 × 250 × 16 × 30	H600 × 250 × 12 × 20
L27~L31	300	10	C50	Q355	H1000 × 250 × 20 × 35	H800 × 250 × 15 × 25	250	10	C50	Q355	H800 × 250 × 16 × 30	H600 × 250 × 12 × 20
L32~L36	250	10	C40	Q355	H750 × 250 × 15 × 25	H600 × 250 × 10 × 15	250	10	C40	Q355	H700 × 250 × 14 × 25	H500 × 250 × 12 × 20
L37~L41	250	10	C40	Q355	H500 × 250 × 10 × 20	H400 × 200 × 8 × 15	250	10	C40	Q355	H500 × 250 × 10 × 20	H400 × 250 × 8 × 15
L42~L46	250	10	C40	Q355	H500 × 250 × 10 × 20	H400 × 200 × 8 × 15	250	10	C40	Q355	H500 × 250 × 10 × 20	H400 × 250 × 8 × 15

Note: (1) Steel plate thickness of exterior wall t_{SE}, steel plate thickness of interior wall t_{SI}; (2) The cross-sectional dimensions and material information of the frame beams and columns in this model are consistent with BM-7.5-C-P; (3) The steel grade of the non-energy dissipation beam section of the replaceable energy dissipation coupling beam is Q355, and the steel grade of the energy dissipation beam section is Q235.

3.2. Main Design Results

The elastic time history analysis employs the vibration mode-decomposition response spectrum method, with a damping ratio of 4% assigned to each vibration mode. Table 5 presents the key calculation parameters for BM-7.5-C-P and HP-7.5-C-P. The elastic story drift ratio limits for high-rise concrete structures are determined by interpolation between 1/800 and 1/500 in buildings with heights ranging from 150 m to 250 m, as specified in the Tall Buildings Design Code. Specifically, the model with a height of 198.4 m adheres to a limit of 1/620. For structural systems composed of CFSSTCs, steel beams or composite beams and concrete-filled steel plate shear walls (CFSPSWs), the General Composite Code for Composite Structures (GB55004-2021) [33] (hereinafter referred to as the General Composite Code) stipulates that the elastic story drift ratio limit is 1/250. In summary, the design results of both models meet the requirements of China's structural design specifications.

Table 5. The main calculation indexes of BM-7.5-C-P and HP-7.5-C-P.

Model		BM-7.5-C-P	HP-7.5-C-P
Total structural mass (ton)		123,973	112,681
Period (s)	T_1	4.53	5.46
	T_2	4.52	5.43
	T_3	2.72	3.97
	T_4	1.20	1.72
	T_5	1.19	1.70
	T_6	0.99	1.56
Maximum story drift ratio		1/726	1/529
Maximum frame–shear ratio		11.7%	17.6%
Bottom frame overturning moment ratio		16.0%	22.7%
Stiffness–weight ratio		2.03	1.52

3.3. Establishment and Verification of Elastoplastic Model

The SSG models of BM-7.5-C-P and HP-7.5-C-P were established, being designated as BM-7.5-C-S and HP-7.5-C-S, respectively. In this paper, mode damping is adopted in the elastoplastic analysis. The damping ratio of each mode in the elastic stage of the structure is 4%. As the structure transitions into the plastic stage, damping is manifested through the nonlinear behavior exhibited by the material. Shear walls, reinforced concrete coupling beams, and slabs are modeled using elastoplastic-layered shell elements, while columns, reinforced concrete beams, and H-shaped steel beams utilize fiber bundle Timoshenko beam elements. The concrete constitutive model adopts the elastoplastic damage model, which can consider the differences in tensile and compressive strength of the concrete materials, stiffness, and strength degradation, as well as the stiffness recovery presented by the closure of tensile and compressive cyclic cracks. The nonlinear material model of steel adopts a bilinear kinematic hardening model.

Modal analysis was performed on the SSG models and the primary calculation indexes were compared with those obtained from PKPM analysis. The errors of the total mass and the first six periods calculated by both the SSG model and the PKPM model for both structures are controlled within 3% shown in Table 6, indicating that the SSG models demonstrate reasonable accuracy, thus making them suitable for subsequent calculation and analysis.

3.4. Ground Motion Selection

This paper focuses more on the elastoplastic situation of structures during MCEs. Therefore, an elastic model is used for ground motion selection, with a damping ratio of 5% equivalent to the level of MCEs. In theory, the damping ratio closed to the elastoplastic damping ratio of the structure under MCEs is the best. Based on the design earthquake and site classes of the research object, eight sets of natural waves were selected from the strong earthquake record database, and three sets of artificial waves (RGB01, RGB02, and RGB03)

were generated. The information of the natural waves selected in the paper is shown in Table 7. A total of 11 sets of ground motion records were utilized as seismic inputs, with each set comprising two horizontal components and one vertical component of seismic waves. The number of seismic motions selected in this paper meets the requirements of seven sets in the Seismic Design Code, as well as meets the requirements of 11 sets in the Resilience Standard for the seismic resilience assessment of structures.

Table 6. Comparison of the results between SSG model and PKPM model.

Type		Conventional Model			High-Performance Model		
Software Model		PKPM BM-7.5-C-P	SSG BM-7.5-C-S	PKPM/SSG	PKPM HP-7.5-C-P	SSG HP-7.5-C-S	PKPM/SSG
Mass (ton)		123,973	125,287	0.99	112,681	114,544	0.98
Period (s)	T_1	4.53	4.46	1.01	5.46	5.52	0.99
	T_2	4.52	4.42	1.02	5.43	5.46	1.00
	T_3	2.72	2.70	1.01	3.97	3.99	0.99
	T_4	1.20	1.20	1.00	1.72	1.69	1.02
	T_5	1.19	1.18	1.02	1.70	1.65	1.03
	T_6	0.99	0.98	1.02	1.56	1.52	1.02

Table 7. The information of the natural waves.

Name	Type	Event	Date	Station	Mag (ML)	Rjb (km)	Vs30 (m/s)
TH001	Natural wave from PEER ground motion database	Cape Mendocino	25 April 1992	Fortuna Blvd	7.01	19.95	457.06
TH054		Darfield New Zealand	9 March 2010	WSFC	7	26.93	344.02
TH057		El Mayor-Cucapah	4 April 2010	El Centro—Meadows Union School	7.2	28.3	276.25
TH060		Imperial Valley-06	15 October 1979	Parachute Test Site	6.53	12.69	348.69
TH064		Irpinia Italy-01	23 November 1980	Auletta	6.9	9.55	476.62
TH074		Iwate	13 June 2008	Nakashinden Town	6.9	40.98	436.34
TH091		Loma Prieta	18 October 1989	Sunnyvale—Colton Ave.	6.93	24.23	267.71
TH101		Parkfield	28 June 1966	Cholame—Shandon Array 12	6.19	17.64	408.93

The ratio of the base shear force calculated by elastic time history analysis to that obtained from the mode-decomposition response spectrum method of the two models under each group of seismic input ranges from 0.76 to 1.21. The ratio of the average base shear force to that obtained from the response spectrum for 11 sets of ground motion records is 99% for BM-7.5-C-P and 97% for HP-7.5-C-P, satisfying the requirements stated in Article 5.1.2 of the Seismic Design Code. Detailed data are shown in Table 8. The main direction acceleration response spectrum of the ground motion records for each set is depicted in Figure 4, along with a comparative analysis of the average response spectrum against the normative design response spectrum.

Table 8. Ground motion selection results for the two models.

Model		BM-7.5-C-P		HP-7.5-C-P	
		Base Shear Force (kN)	Ground Motion/ Response Spectrum	Base Shear Force (kN)	Ground Motion/ Response Spectrum
Response spectrum		1.31×10^5	100%	1.05×10^5	100%
Ground motion	TH001	1.59×10^5	121%	9.29×10^4	88%
	TH054	1.39×10^5	106%	1.02×10^5	97%
	TH057	1.08×10^5	82%	1.06×10^5	101%
	TH060	1.49×10^5	114%	9.13×10^4	87%
	TH064	1.24×10^5	95%	1.08×10^5	103%
	TH074	1.06×10^5	81%	7.94×10^4	76%
	TH091	1.58×10^5	121%	9.15×10^4	87%
	TH101	1.24×10^5	95%	1.00×10^5	95%
	RGB01	1.28×10^5	98%	1.14×10^5	109%
	RGB02	1.25×10^5	95%	1.18×10^5	112%
	RGB03	1.13×10^5	86%	1.12×10^5	107%
Average value		1.30×10^5	99%	1.01×10^5	97%

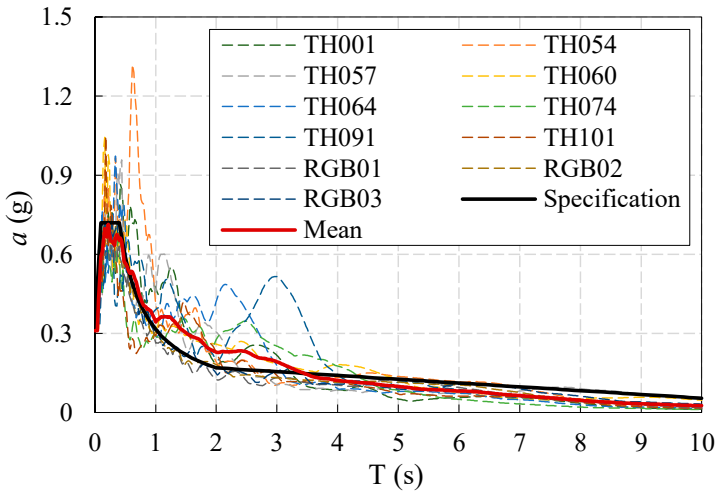

Figure 4. Structural response spectrum.

4. Elastoplastic Analysis under MCEs

The seismic input for the elastoplastic analysis under MCEs in this paper is a three-dimensional input. The ratio of peak ground acceleration (PGA) in three directions is 1:0.85:0.65 (main direction: secondary direction: vertical), and the PGA of the main direction is 0.31 g. The specific analysis results are as follows.

4.1. Story Displacement and Story Drift Ratio

The average values of the story displacement envelope and story drift ratio envelope of the two models (BM-7.5-C-S and HP-7.5-C-S) under the input ground motions are shown in Figure 5. It can be observed that the story displacement and story drift ratio responses in the lower part of the two models are relatively close. However, in the middle upper part, the story displacement and story drift ratio of BM-7.5-C-S are smaller than those of HP-7.5-C-S.

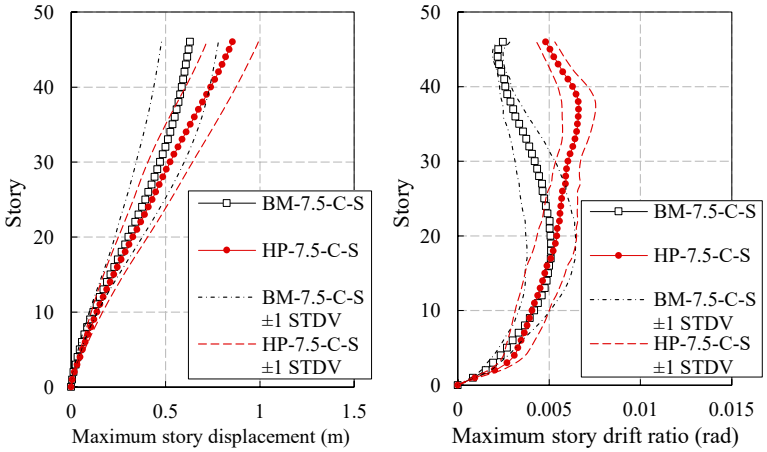

(**a**) Story displacement (**b**) Story drift ratio

Figure 5. The average values of the story displacement envelope and story drift ratio envelope.

According to the Seismic Design Code and the General Composite Code, the story drift ratio limit of BM-7.5-C-S under MCEs is 1/100, and the story drift ratio limit of HP-7.5-C-S is 1/50. The analysis results indicate that the story drift ratio of both models under MCEs complies with the code requirements. The ratios of the plastic story drift ratio limits corresponding to BM-7.5-C-S and HP-7.5-C-S to their corresponding maximum story drift ratios are 2.0 and 3.0, respectively. It can be seen that, under MCEs, the story drift ratio of HP-7.5-C-S has a higher redundancy than that of BM-7.5-C-S compared to the specification limits. In summary, the high-performance structural system demonstrates a superior performance in assessing the story drift ratio during MCEs.

4.2. Development of Structural Plasticity

The structural damage varies under different seismic inputs. Based on the results of finite element analysis, significant plastic deformation is observed in both models when subjected to natural wave TH054. Therefore, taking the TH054 seismic condition as an example, this study introduces the plastic development of the core tube and outer frame in both models under MCEs. The plastic development of the core tube of BM-7.5-C-S and HP-7.5-C-S is shown in Figures 6 and 7, respectively. For concrete components in the figure, the label represents the compressive damage factor. For steel components, the label represents the ratio of the maximum stress to the yield stress of the component. The steel in the outer frames of both models remains within its elastic limit, and the concrete compression damage factor is within 0.1. The outer frame is basically intact, and no further elaboration will be provided subsequently.

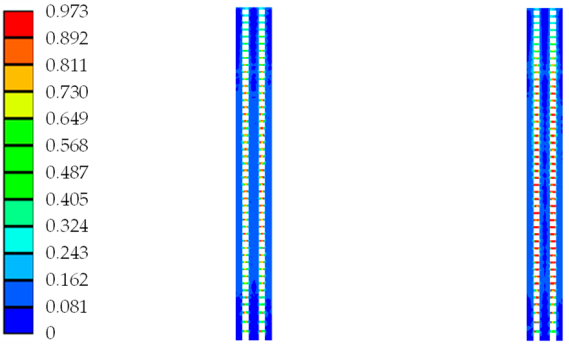

(**a**) Label (**b**) Exterior wall damage (**c**) Interior wall damage

Figure 6. The plastic development of the core tube of BM-7.5-C-S.

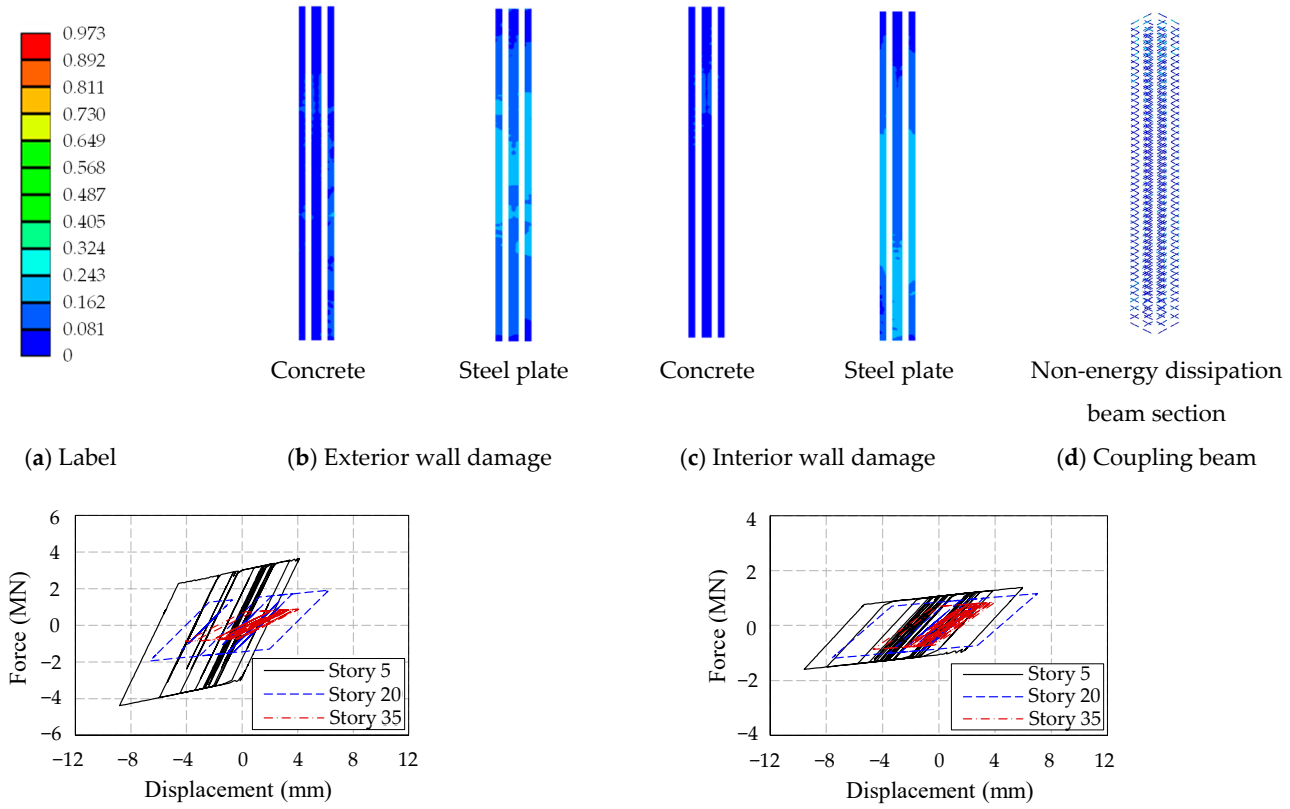

(**a**) Label (**b**) Exterior wall damage (**c**) Interior wall damage (**d**) Coupling beam

(**e**) Hysteretic behavior of coupling beam of exterior wall (**f**) Hysteretic behavior of coupling beam of interior wall

Figure 7. The plastic development of the core tube of HP-7.5-C-S.

The compression damage factor of most shear walls in BM-7.5-C-S is below 0.1, indicating minimal structural deterioration; however, over 50% of the coupling beams exhibit a compression damage factor exceeding 0.3, indicating that many of the coupling beams have entered the plastic energy dissipation stage, which could effectively dissipate the seismic energy and minimize damage to primary components such as shear walls. Consequently, the seismic response results of the coupling beams also satisfy the requirements of seismic performance objectives. The concrete in the majority of HP-7.5-C-S shear walls remains undamaged, with the stress level of the steel plate being maintained at a low values, well within 30% of its yield stress limit, while ensuring that all components remain essentially intact. The non-energy dissipation beam section of the replaceable energy dissipation coupling beam is in an elastic working state, satisfying the design requirements. The energy dissipation beam section is capable of effectively dissipating energy, exhibiting a complete hysteretic curve during seismic events.

4.3. Structural Stiffness Degradation

As the seismic response increases, the structure gradually enters plasticity, resulting in the overall stiffness deterioration and an extended period. Therefore, after the elastoplastic time history analysis of the structure, the mode analysis can be performed to quantitatively evaluate the stiffness degradation of the structure by analyzing the extension of the structural fundamental period. According to the relationship between the period and stiffness, the degradation rate D_{Ki} of a certain order of stiffness can be calculated by the following equation:

$$D_{\mathrm{Ki}} = 1 - \left(T_{\mathrm{i}}/T_{\mathrm{i}}'\right)^2 \quad (1)$$

In the formula, T_{i} is the i-th order period of the structure before the earthquake, and T_{i}' is the i-th order period of the structure after the earthquake.

The first-order stiffness degradation rates of the two models are shown in Table 9. The average stiffness degradation rates of BM-7.5-C-S and HP-7.5-C-S are 0.09 and 0.02, respectively. It can be observed that the stiffness degradation of the high-performance structural system is significantly smaller than that of the conventional structural system, indicating that the high-performance structural system has a better seismic performance.

Table 9. The first-order stiffness degradation rates.

Ground Motion Records	BM-7.5-C-S		HP-7.5-C-S	
	T_1'	$1-(T_1/T_1')^2$	T_1'	$1-(T_1/T_1')^2$
TH001	4.52	0.03	5.66	0.05
TH054	4.79	0.13	5.64	0.04
TH057	4.49	0.01	5.70	0.06
TH060	4.84	0.15	5.48	-0.02
TH064	4.51	0.02	5.52	0.00
TH074	4.48	0.01	5.61	0.03
TH091	4.79	0.13	5.59	0.02
TH101	4.72	0.11	5.54	0.01
RGB01	4.81	0.14	5.62	0.03
RGB02	4.76	0.12	5.52	0.00
RGB03	4.81	0.14	5.61	0.03
Average value	4.68	0.09	5.59	0.02

4.4. Assessment of the Function of the Second Line of Defense of the Outer Frame

The core tube, serving as the first defensive barrier in frame–core tube super-tall buildings, may incur severe damage during intense seismic events. The subsequent redistribution of internal forces will result in a significant seismic impact on the outer frame. Therefore, an appropriate proportion of stiffness between the core tube and the outer frame is necessary to effectively serve as the second line of defense of the outer frame. The effect of the second line of defense can be evaluated using the frame–shear ratio (frame layer shear force/base shear force) and the frame overturning moment ratio (frame overturning moment/total overturning moment). The calculation results are shown in Figure 8.

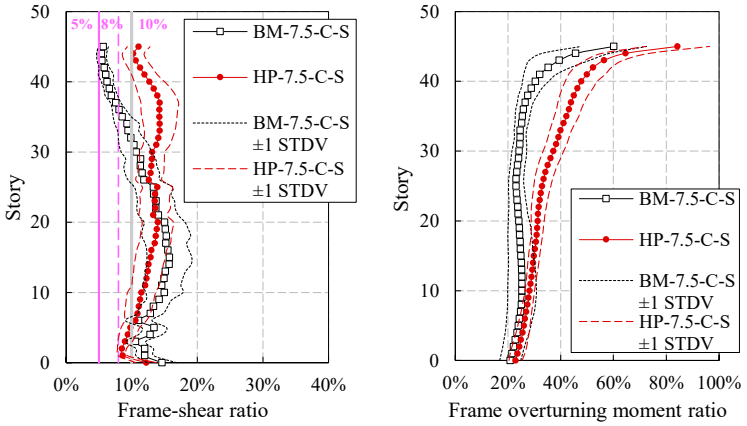

(**a**) Frame–shear ratio (**b**) Frame overturning moment ratio

Figure 8. The calculation results of BM-7.5-C-S and HP-7.5-C-S.

According to the 2015 edition of the Technical Key Points for Special Review of Seismic Fortification of Tall Building Engineering [18] (hereinafter referred to as the Technical Key Points), it is stipulated that the story shear force allocated by the outer frame, except for individual stories at the bottom, strengthened stories and theirs upper and lower stories, and should generally be no less than 8% of the base shear force, with a maximum value that is no lower than 10%, and a minimum value that is no lower than 5%. The maximum

frame–shear ratio of both models exceeds 10%, with the minimum value surpassing 5%. The proportion of stories with a frame–shear ratio exceeding 8% is 80.4% for BM-7.5-C-S and 100% for HP-7.5-C-S. In summary, the frame–shear ratio of each model satisfies the requirements stated in the Technical Key Points, and HP-7.5-C-S exhibits better performance.

The frame overturning moment ratio of the bottom frame under MCEs for BM-7.5-C-S and HP-7.5-C-S is 20.9% and 22.9%, respectively, representing an increase of 30.3% and 1.0% compared to the results obtained from seismic analysis under SLEs. The findings suggest that the function of the second line of defense of the high-performance structural system exhibits a slightly superior strength compared to that of the conventional structural system. Concurrently, as structural plasticity advances, the function of the second line of defense within the frame is further enhanced, thereby highlighting the merits of a dual system. It is noteworthy that the increase in the overturning moment ratio of the bottom frame of the HP-7.5-C-S is merely 1%, which, to some extent, indicates that the plastic damage of the core tube and the overall stiffness degradation of the structure are relatively minor under MCEs. The conclusion can be mutually corroborated by the analysis findings presented in Sections 4.2 and 4.3.

5. Seismic Resilience Assessment

5.1. Assessment Process

Utilizing the seismic resilience assessment program developed by the research group [29] in accordance with the Resilience Standard, the seismic resilience assessment of various structural models can be carried out. The specific assessment process is shown in Figure 9. For a given structural model, first determine the basic information of buildings and their components (type, quantity and vulnerability data), and select no fewer than 11 sets of ground motion records based on the design earthquake and site classes. Subsequently, a three-dimensional seismic input should be used to perform a nonlinear time history analysis on the structural model in order to generate the original engineering demand parameter matrix. The seismic resilience assessment of the building can be carried out when the average value of the residual story drift ratio satisfies the 0.5% limit requirement specified in the Resilience Standard.

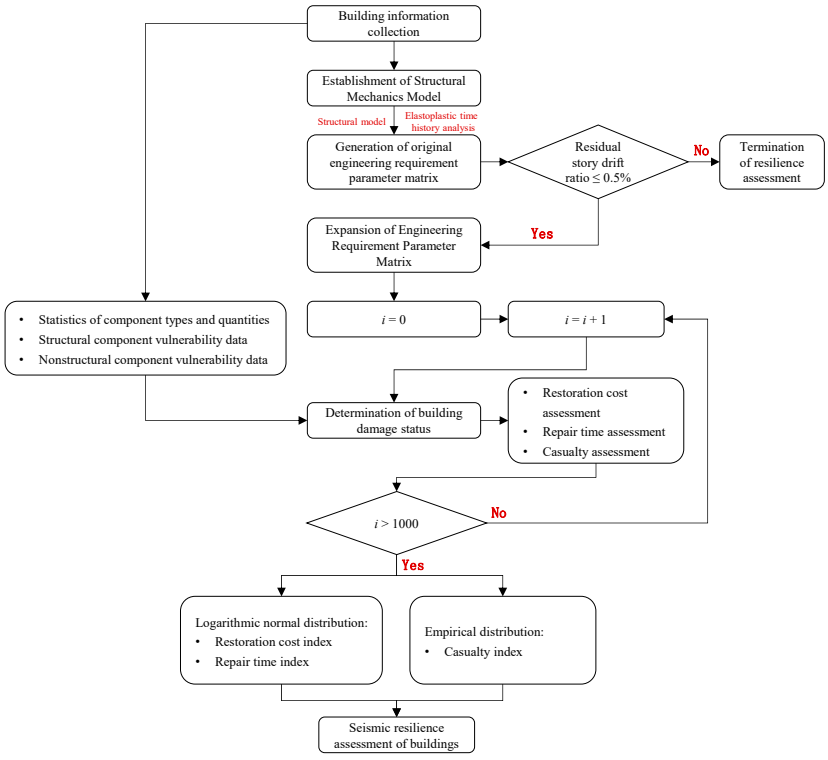

Figure 9. Seismic resilience assessment process of buildings.

To enhance the robustness of the assessment results, the Monte Carlo simulation method is adopted to expand the engineering demand parameter matrix, ensuring that the expanded engineering demand parameters possess identical joint distribution and probability distribution parameters as those in the original engineering demand parameter matrix. In a Monte Carlo simulation, the damage state of components is determined through random number generation, in conjunction with the exceeding probability of various damage states of the components, and the seismic resilience assessment index of buildings (restoration cost, repair time, and casualty) can be calculated. The resilience standard stipulates that the number of simulations should be 1000 times or more. The seismic resilience assessment index adopts the fitting values with an 84% guarantee rate calculated by the Monte Carlo simulation method. Specifically, the restoration cost index and repair time index are fitted using a logarithmic normal distribution model recommended by the resilience standard, while the distribution of the casualty index deviates from a logarithmic normal distribution, thus requiring an empirical distribution model for fitting [34].

Finally, the seismic resilience assessment level of buildings should be comprehensively evaluated based on the three seismic resilience assessment indexes, and the lowest level of the three indexes should be taken as the seismic resilience assessment level of buildings.

The determination of the seismic resilience assessment level of buildings is divided into two stages [35]: (1) In the first stage, the seismic resilience assessment of buildings under DBEs should be carried out. If it satisfies the criteria for one-star resilient buildings, the assessment can progress to the subsequent stage; otherwise, the assessment should be terminated; (2) In the second stage, conduct seismic resilience assessment for buildings under MCEs, and update the building's seismic resilience assessment level if it meets the criteria for two-star or three-star resilient buildings; otherwise, maintain the original one-star resilience rating.

5.2. Value of Vulnerability Parameters for Composite Components

The structural models for seismic resilience comparison in this section include CFSSTCs, CFSPSWs, and steel-reinforced concrete shear walls. The recommended values for the vulnerability parameters of these components are not provided in the Resilience Standard. Among them, for steel-reinforced concrete shear walls, Cui [29] provided the recommended values for the seismic resilience assessment based on the existing literature experimental data. Therefore, this paper adopts the above-recommended values as the vulnerability parameter of steel-reinforced concrete shear walls. Due to the lack of relevant literature for the statistical analysis of the test data pertaining to CFSSTCs and CFSPSWs, this study undertakes a comprehensive collection and organization of experimental data from existing sources in order to determine their vulnerability parameters. The specific steps are as follows:

(1) Based on experimental reported data in the literature, calculate the rotation angles of the components corresponding to the nominal yield point, peak point, and limit point, namely θ_y, θ_p, and θ_u;
(2) Assuming that the experimental data adhere to a logarithmic normal distribution, calculate the logarithmic mean and logarithmic standard deviation of the experimental data under various rotation angles, and determine the corresponding logarithmic normal distribution function;
(3) Calculate the correlation coefficient R between the experimental data and the fitted data determined based on the logarithmic normal distribution. If $R > 0.8$, this indicates a strong correlation between the experimental data and the fitted data, and the assumption of a logarithmic distribution is valid;
(4) Determine the median value and logarithmic standard deviation for each limit state of the component based on the characteristics of the logarithmic normal distribution.

This paper collected relevant literature and summarized the seismic experimental data of 56 CFSSTCs [36–44] and 25 CFSPSWs [16,45–48]. Subsequently, statistical analysis was conducted separately for the parameters θ_y, θ_p, and θ_u of CFSSTCs and CFSP-

SWs. The experimental data exhibit a logarithmic normal distribution, as illustrated in Figures 10 and 11. The correlation coefficient between the experimental data and the fitting data of each limit rotation angle of various components exceeds 0.93, indicating that each group of experimental data conforms to the logarithmic normal distribution. The vulnerability parameters of CFSSTCs and CFSPSWs are presented in Table 10.

Table 10. The vulnerability parameters of CFSSTCs and CFSPSWs.

Skeleton Line Parameters	CFSSTC		CFSPSW	
	Median Value	Logarithmic Standard Deviation	Median Value	Logarithmic Standard Deviation
θ_y	0.0103	0.48	0.0075	0.28
θ_P	0.0249	0.37	0.0167	0.28
θ_u	0.0401	0.40	0.0221	0.34

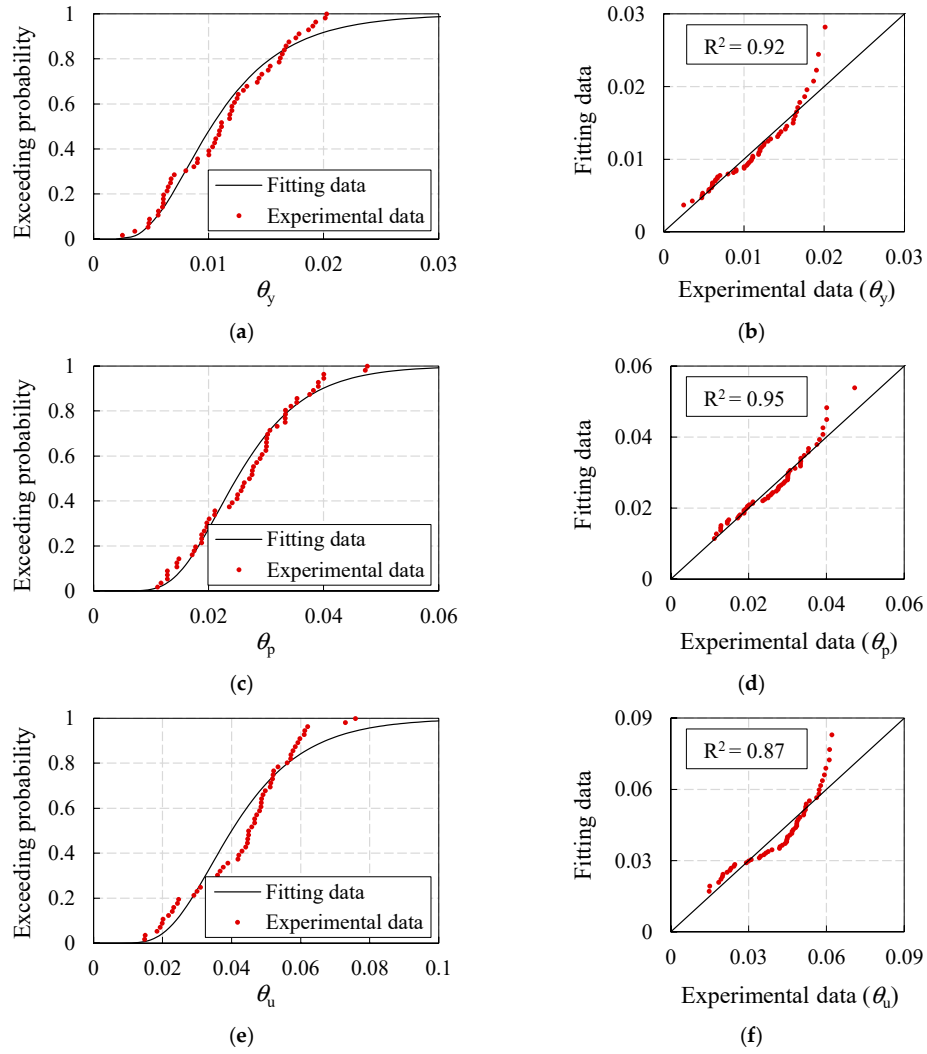

Figure 10. Comparison between the experimental data and fitting data of CFSSTCs. (**a**) Damage state (θ_y). (**b**) The correlation coefficient between the experimental data and the fitting data (θ_y). (**c**) Damage state (θ_p). (**d**) The correlation coefficient between the experimental data and the fitting data (θ_p). (**e**) Damage state (θ_u). (**f**) The correlation coefficient between the experimental data and the fitting data (θ_u).

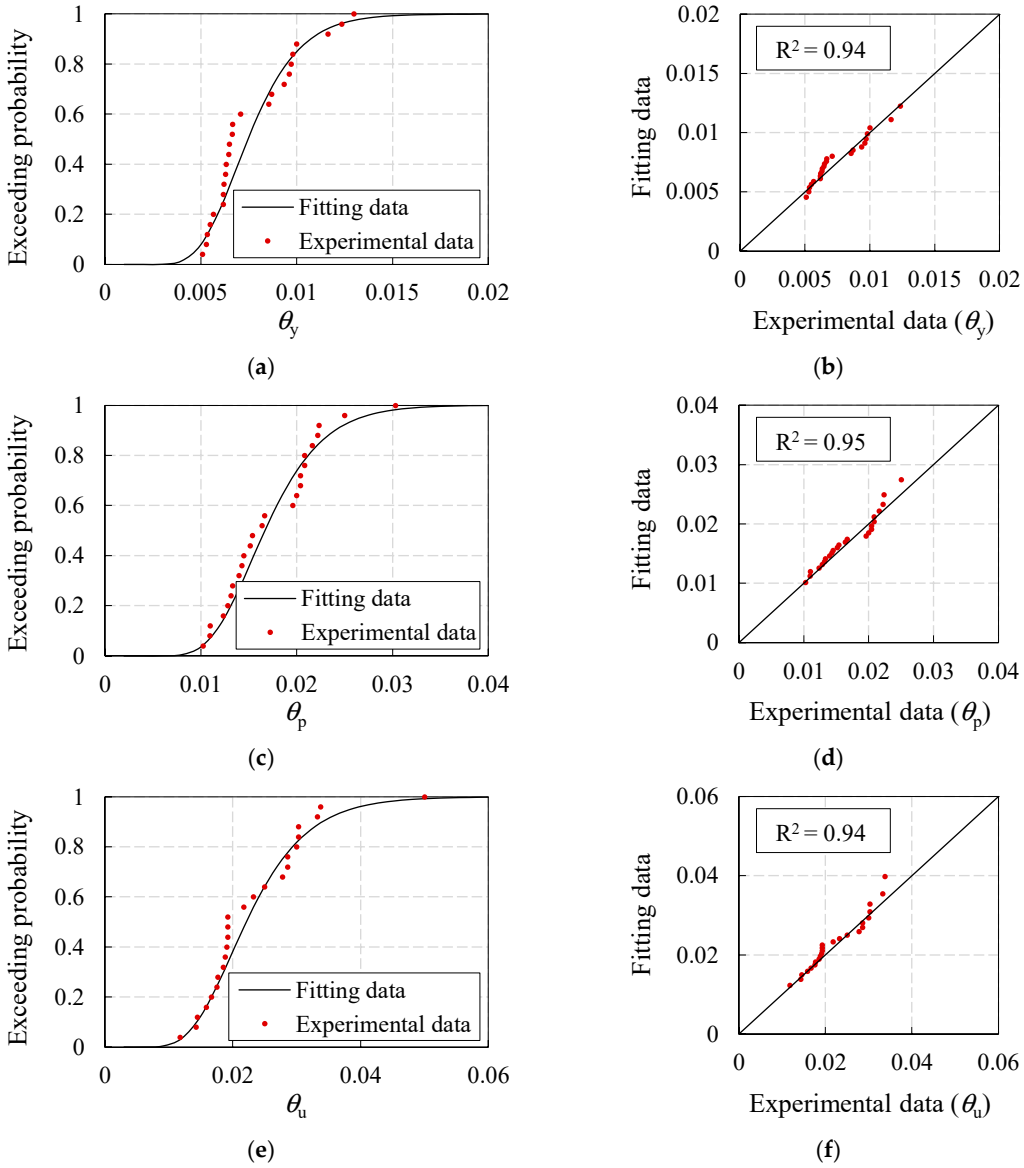

Figure 11. Comparison between experimental data and fitting data of CFSPSWs. (**a**) Damage state (θ_y). (**b**) The correlation coefficient between the experimental data and the fitting data (θ_y). (**c**) Damage state (θ_p). (**d**) The correlation coefficient between the experimental data and the fitting data (θ_p). (**e**) Damage state (θ_u). (**f**) The correlation coefficient between the experimental data and the fitting data (θ_u).

5.3. Comparison of Seismic Resilience Assessment Results

This section conducted seismic resilience assessment for both conventional and high-performance models under DBEs and MCEs, and the assessment results (restoration cost index κ, repair time index T_{tot}, injury rate γ_H, and death rate γ_D) are shown in Table 11. The specific conclusions are as follows:

(1) Under DBEs, the seismic resilience assessment results of both models are one-star, and all indexes are superior to the assessment standards. Notably, the high-performance model demonstrated a better performance across all indexes;

(2) Under MCEs, the seismic resilience assessment results of both models are two-star. The restoration cost index of both models can reach a three-star rating, and the repair time index can reach a two-star rating. The high-performance model has better indexes. The casualty index exhibits a significant disparity between the two models,

with the high-performance model achieving a three-star rating while the conventional model attains a two-star rating;

(3) The conventional model already has good seismic resilience. For the high-performance model, the core tube is constructed with high-performance CFSPSWs and replaceable energy dissipation coupling beams, thereby enhancing the seismic resilience assessment indexes under DBEs and MCEs. The restoration cost index, repair time index, injury rate, and death rate under the MCEs of the high-performance model are 62.2%, 84.7%, 4.9%, and 0% of those of the conventional model, respectively. Therefore, the high-performance models can better enhance the safety of individuals' lives and assets.

Table 11. Comparison of the seismic resilience assessment results of the two models under DBEs and MCEs.

Model		Conventional Model		High-Performance Model	
		Index	Assessment	Index	Assessment
DBE	κ	0.70%	One-star	0.50%	One-star
	T_{tot}	13.8d	One-star	13.2d	One-star
	γ_H	2.8×10^{-5}	One-star	2.5×10^{-6}	One-star
	γ_D	0		0	
	Assessment	One-star		One-star	
MCE	κ	3.70%	Three-star	2.30%	Three-star
	T_{tot}	19.0d	Two-star	16.1d	Two-star
	γ_H	3.5×10^{-4}	Two-star	1.7×10^{-5}	Three-star
	γ_D	5.4×10^{-5}		0	
	Assessment	Two-star		Two-star	
Assessment		Two-star		Two-star	

Currently, the impact of EREs on building structures is not considered in China's seismic design system. However, given the complexity and uncertainty of earthquakes, it is plausible for structures to encounter EREs during their intended lifespan. During the 1976 Tangshan earthquake, Tangshan had a seismic fortification intensity of 6 degrees (currently, it is 8 degrees), and the epicenter recorded an intensity of 11 degrees. The 2008 Wenchuan earthquake had a fortification intensity of 7 degrees and the actual intensity of the epicenter reached 11 degrees. Therefore, it is imperative to investigate the seismic resilience of super-tall buildings under EREs. This paper compares the seismic resilience assessment levels of two models under an ERE condition of 510 gal, and the assessment results are shown in Table 12. The component damage state level, restoration cost, repair time, injury rate, and death rate of each story of each model are shown in Figures 12 and 13. Among them, the component damage state level is evaluated based on the percentile value with an 84% guarantee rate obtained from 1000 Monte Carlo simulation results. The specific conclusions are as follows:

(1) Based on the story distribution diagram of component damage state levels shown in Figure 12a, it is evident that, under EREs, the conventional model experiences concentrated damage in the core tube. Additionally, shear walls exhibit a damage state level exceeding 3, while coupling beams exhibit a damage state level exceeding 2. The overall damage of the high-performance model is relatively small, and the damage state level of each component is less than level 2, as shown in Figure 13a.

(2) Under EREs, the final seismic resilience assessment result of the conventional model is zero-star, while that of the high-performance model is two-star. Among them, the repair time index of the conventional model is two-star, while the other indexes are zero-star. The restoration cost index and repair time index of the high-performance model are two-star, and the casualty index is three-star, as shown in Table 12. The restoration cost index, repair time index, injury rate, and death rate of the high-performance model are 51.8%, 69.4%, 2.0%, and 0.4% of those of the conventional model, respectively.

Table 12. Comparison of seismic resilience assessment results of the two models under EREs.

Model		Conventional Model		High-Performance Model	
		Index	Assessment	Index	Assessment
ERE	k	11.00%	Zero-star	5.70%	Two-star
	T_{tot}	29.1d	Two-star	20.2d	Two-star
	g_H	2.5×10^{-3}	Zero-star	5.0×10^{-5}	Three-star
	g_D	4.4×10^{-4}		1.6×10^{-6}	
Assessment		Zero-star		Two-star	

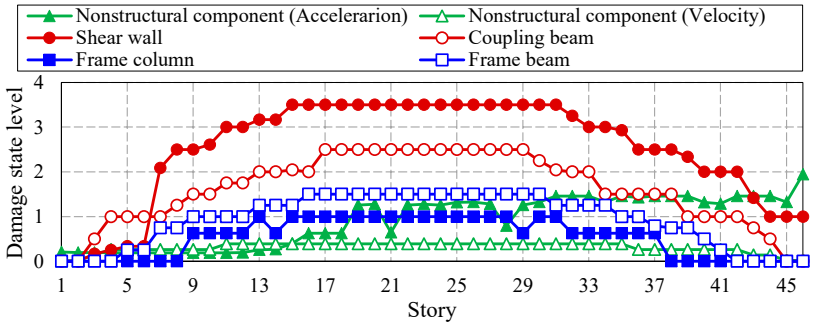

(**a**) Component damage state level

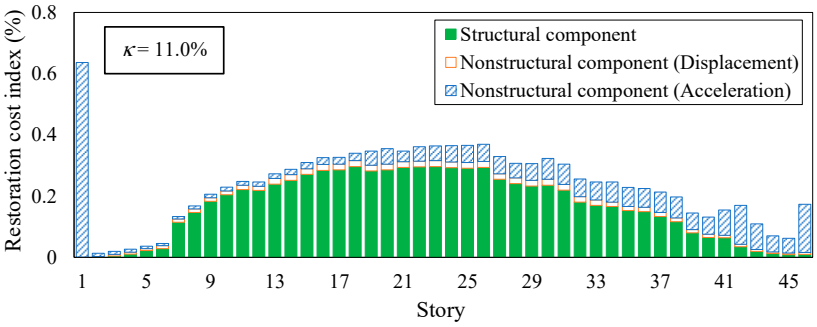

(**b**) Restoration cost index

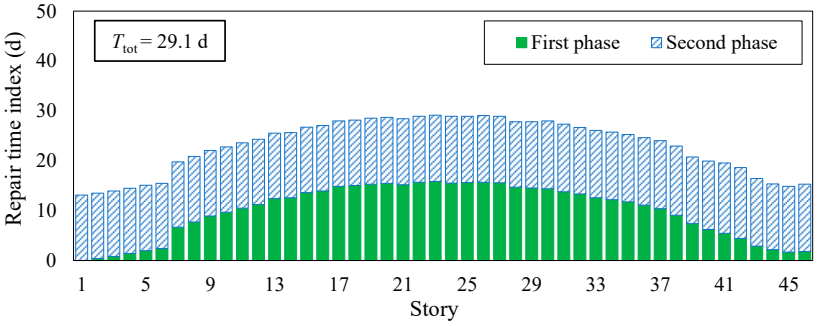

(**c**) Repair time index

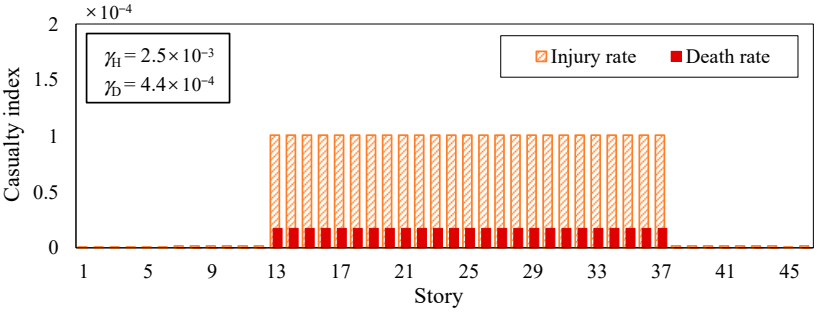

(**d**) Casualty index

Figure 12. Seismic resilience assessment results of the conventional model under EREs (510 gal).

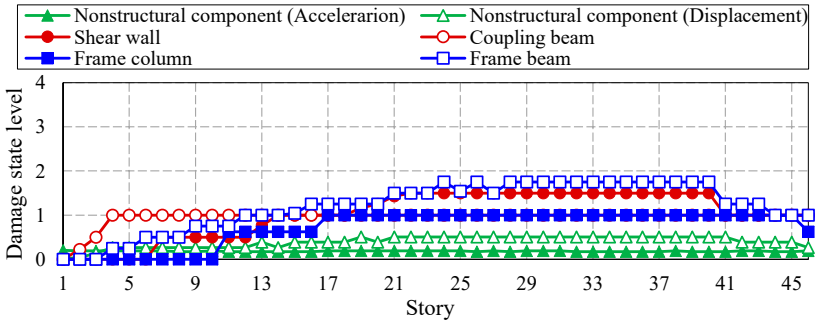

(**a**) Component damage state level

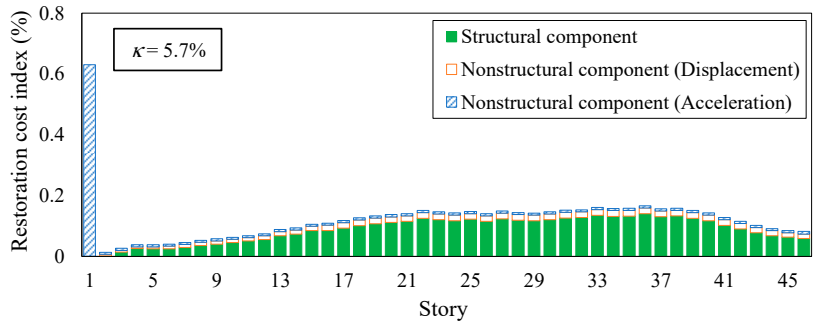

(**b**) Restoration cost index

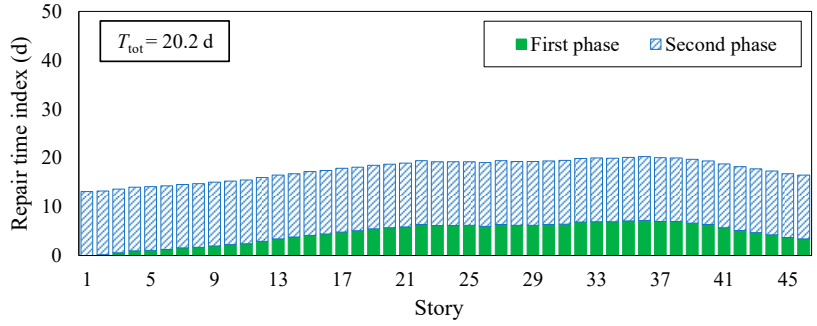

(**c**) Repair time index

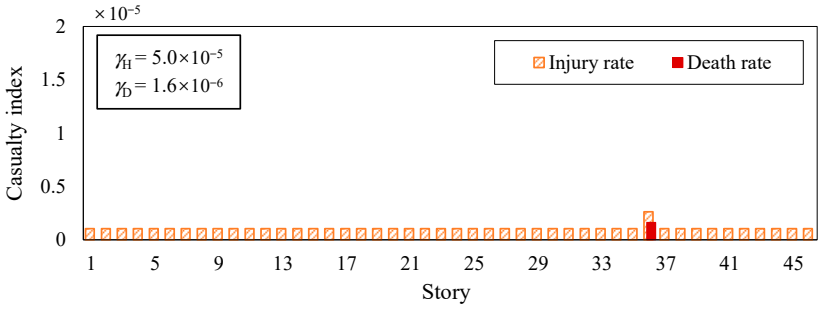

(**d**) Casualty index

Figure 13. Seismic resilience assessment results of the high-performance model under EREs (510 gal).

In conclusion, the high-performance model demonstrates a superior seismic resilience under various earthquake conditions. Furthermore, as the earthquake intensity escalates, the seismic resilience of the high-performance model is significantly enhanced compared to the conventional model, especially in terms of mitigating casualties, as depicted in Figure 14.

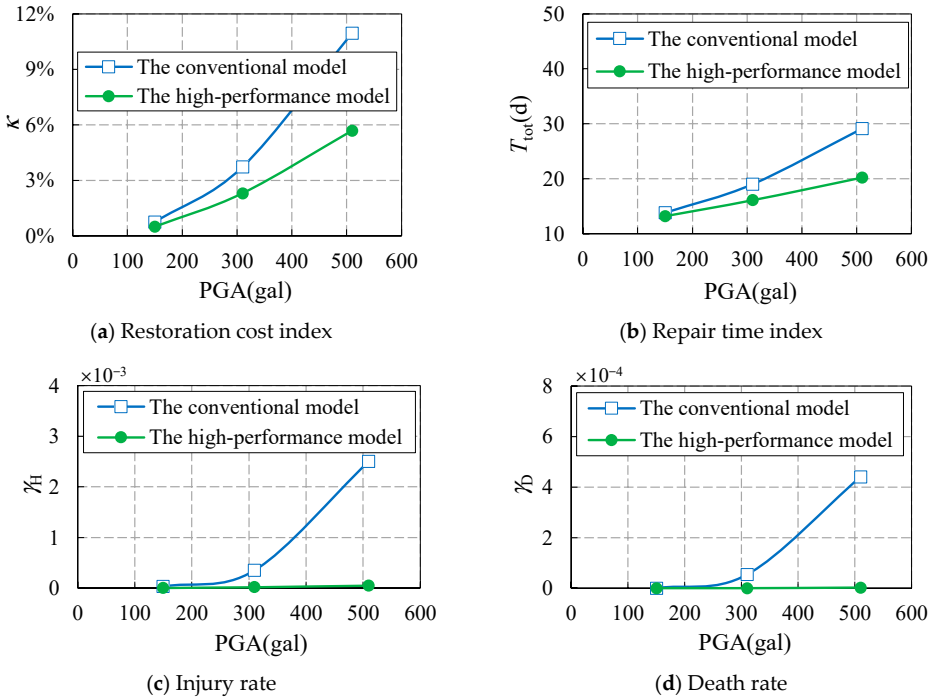

(**a**) Restoration cost index (**b**) Repair time index

(**c**) Injury rate (**d**) Death rate

Figure 14. The comparison of seismic resilience assessment indexes of the two models under various earthquake conditions.

6. Conclusions

The paper proposed a composite frame—high-strength steel plate wall core tube resilient structural system, and designed two 200 m level frame–core tube models: the conventional model and the high-performance model. The corresponding elastoplastic analysis models were established to compare the seismic performance of each model under MCEs, as well as the seismic resilience under DBEs, MCEs, and EREs. The effectiveness of the proposed novel high-performance structural system has been validated. The key findings of this paper are as follows:

(1) In comparison to the conventional model, the high-performance model can effectively optimize the thickness of the shear walls, reduce the structural self-weight, and maximize the usable space in the buildings. Although there is a slight reduction in the overall stiffness and an increase in the period, these changes remain within acceptable limits that meet design requirements.

(2) Under MCEs, the high-performance model exhibits a higher redundancy in terms of the story drift ratio, lower plastic damage and overall stiffness degradation of the structure, and a better seismic performance compared to the conventional model. In addition, the performances of both models meet the requirements of the technical key points in terms of the frame–shear ratio, with the high-performance model demonstrating superior capabilities. Meanwhile, the overturning moment ratio of the bottom frame of both models exceeds 20%, which indicates that the outer frame can achieve the function of the second line of defense.

(3) The vulnerability parameters of CFSSTCs and CFSPSWs are calibrated in this study through a systematic collection and organization of experimental data from existing literature, thereby providing fundamental data for the seismic resilience assessment of the novel high-performance structural systems.

(4) Both the conventional model and the high-performance model exhibit a seismic resilience rating of two stars; however, the high-performance model outperforms the conventional one across all assessment indexes. Under EREs, the seismic resilience assessment level of the high-performance model is still two-star, while that of the conventional model is zero-star. The seismic resilience of the high-performance

model is optimal under various earthquake conditions. Simultaneously, with the increasing earthquake intensity, the high-performance model exhibits significantly enhanced seismic resilience compared to the conventional model, particularly in terms of minimizing casualties and safeguarding human lives and property.

The above conclusions are drawn from the seismic response analysis of the frame-core structures at the 200 m level, which were designed based on specific seismic intensity. Further research efforts are required to explore the applicability of the new structural system in high-performance structural systems with varying heights and seismic intensities, based on the findings of this current study. The subsequent research work should also address the carbon dioxide emissions and engineering economic benefits associated with high-performance structural systems.

Author Contributions: Conceptualization, C.W. and C.C.; methodology, L.Z.; software, M.C.; resources, C.C.; writing—original draft preparation, L.Z.; investiation, L.Z. and M.C.; writing—review and editing, C.W., C.C. and M.C.; supervision, C.C. and C.W. All authors have read and agreed to the published version of the manuscript.

Funding: In this paper: the research was sponsored by the National Key Research and Development Program of China (Grant No. 2022YFC3802000).

Data Availability Statement: Data presented in this research are available upon request from the corresponding author.

Conflicts of Interest: The authors declare no conflicts of interest.

References

1. FEMA. *NEHRP Guidelines and Commentary for Seismic Rehabilitation of Buildings: FEMA 273*; Federal Emergency Management Agency: Washington, DC, USA, 1997.
2. FEMA. *Prestandard and Commentary for the Seismic Rehabilitation of Buildings: FEMA 356*; Federal Emergency Management Agency: Washington, DC, USA, 2000.
3. FEMA. *Next-Generation Performance-Based Seismic Design Guidelines: FEMA 445*; Federal Emergency Management Agency: Washington, DC, USA, 2007.
4. FEMA. *Seismic Performance Assessment of Buildings Volume 1-Methodology, FEMA-P58*; Federal Emergency Management Agency: Washington, DC, USA, 2012.
5. PEER. *Guidelines for Performance-Based Seismic Design of Tall Buildings*; University of California: Berkeley, CA, USA, 2010.
6. Wu, D.; Zhao, B.; Zhu, H. Experimental study on effect of assembly process on seismic performance of modular precast composite shear wall structures. *J. Build. Struct.* **2023**, *80*, 107916. [CrossRef]
7. Xu, L.; Liu, J.; Li, Z. Parametric analysis and failure mode of steel plate shear wall with self-centering braces. *Eng. Struct.* **2021**, *237*, 112151. [CrossRef]
8. Zhou, C.; Wang, J.; Shao, X.; Li, L.; Sun, J.; Wang, X. The feasibility of using ultra-high performance concrete (UHPC) to strengthen RC beams in torsion. *J. Mater. Res. Technol.* **2023**, *24*, 9961–9983. [CrossRef]
9. Huang, H.; Li, M.; Zhang, W.; Yuan, Y. Seismic behavior of a friction-type artificial plastic hinge for the precast beam–column connection. *Arch. Civ. Mech. Eng.* **2022**, *22*, 201. [CrossRef]
10. Huang, H.; Yuan, Y.; Zhang, W.; Li, M. Seismic behavior of a replaceable artificial controllable plastic hinge for precast concrete beam-column joint. *Eng. Struct.* **2021**, *245*, 112848. [CrossRef]
11. Wang, B.; Jiang, H.; Lu, X. Seismic Performance of Steel Plate Reinforced Concrete Shear Wall and Its Application in China Mainland. *J. Constr. Steel Res.* **2017**, *131*, 132–143. [CrossRef]
12. Fan, J.; Ding, R.; Nie, X.; Guo, L.; Yan, J. Research and Application of High-Performance Double Steel-Plate Reinforced Concrete Structures. *J. Build. Struct.* **2022**, *43*, 55–72.
13. Cao, W.; Yu, C.; Dong, H.; Qiao, Q.; Han, L.; Zhang, Y. Experimental Study on Seismic Performance of Composite Shear Walls with Double Steel Plates Under Different Constructions. *J. Build. Struct.* **2013**, *34*, 186–191.
14. Chen, L.; Yin, C.; Wang, C.; Liu, Y. Experimental Study on Seismic Behavior of Double-Skin Composite Wall With L-Shaped Connectors. *J. Constr. Steel Res.* **2020**, *174*, 106312. [CrossRef]
15. He, W.; Wan, Y.; Li, Y.; Bu, J.; Deng, J.; Chen, L.; Zhang, W.; Wen, L. Experimental Study on Seismic Behaviors of The Welded L-Shaped Double Steel Plate-Concrete Composite Shear Wall. *J. Constr. Steel Res.* **2021**, *187*, 106944. [CrossRef]
16. Liu, D.; Shi, Y.; Yu, X. Experimental Study on Seismic Behavior of Modular Composite Shear Wall with Double Steel Plates and Infill Concrete. *Eng. Mech.* **2022**, *39*, 250–260.
17. Wang, K.; Zhang, W.; Chen, Y.; Ding, Y. Seismic Analysis and Design of Composite Shear Wall with Stiffened Steel Plate and Infilled Concrete. *Materials* **2022**, *15*, 182. [CrossRef] [PubMed]

18. Ministry of Housing and Urban-Rural Development of the People's Republic of China (MOHURD). Technical Key Points for Special Review of Seismic Fortification of Tall Building Engineering. 2015. Available online: https://www.mohurd.gov.cn/gongkai/zhengce/zhengcefilelib/201505/20150528_220992.html (accessed on 21 May 2015).
19. *GB/T 51340-2018*; Technical Standard for Steel Plate Concrete Structures of Nuclear Power Plants. China Planning Press: Beijing, China, 2018.
20. Liu, H. Research on the Application of Steel Plate Shear Wall Construction Technology in The Construction of a Super High-Rise Building. *Shanxi Archit.* **2020**, *46*, 77–79.
21. Mao, Z.; Ding, M.; Chen, Z. Structural Design of Steel Frame-Composite Steel Plate Shear Wall in a High-Rise Residential Building. *Build. Struct.* **2020**, *50*, 88–91.
22. Dong, C.; Guo, Q.; Wang, S.; Li, F. Construction Technology of Core Combination Steel Shear Wall in Super High-rise Building Project. *Struct. Constr.* **2021**, *43*, 37–39.
23. Xiao, C.; Li, J.; Lu, Y.; Li, Y. Research on Seismic Performance of Frame-Core Tube Energy Dissipation Structure with C100 High-Strength Concrete. *J. Build. Struct.* **2021**, *42*, 1–9.
24. Jiang, D.; Xiao, C.; Chen, T.; Zhang, Y. Experimental Study of High-Strength Concrete-Steel Plate Composite Shear Walls. *Appl. Sci.* **2019**, *9*, 2820. [CrossRef]
25. Mo, J.; Uy, B.; Li, D.; Thai, H.; Wang, Y. Behaviour and design of composite walls under axial compression. *J. Constr. Steel Res.* **2022**, *199*, 107635. [CrossRef]
26. Hossain, K.; Rafiei, S.; Lachemi, M.; Behdinan, K. Structural performance of profiled composite wall under in-plane cyclic loading. *Eng. Struct.* **2016**, *110*, 88–104. [CrossRef]
27. Chen, L.; Mahmoud, H.; Tong, S.; Zhou, Y. Seismic behavior of double steel plate–HSC composite walls. *Eng. Struct.* **2015**, *102*, 1–12. [CrossRef]
28. Nie, J.; Hu, H.; Fan, J.; Tao, M.; Li, S.; Liu, F. Experimental study on seismic behavior of high-strength concrete filled double-steel-plate composite walls. *J. Constr. Steel Res.* **2013**, *88*, 206–219. [CrossRef]
29. Cui, M. Research on Seismic Performance Evaluation Method of Existing High-Rise Buildings. Ph.D. Thesis, China Academy of Building Research, Beijing, China, 2022.
30. *GB/T 38591-2020*; Standard for seismic Resilience Assessment of Buildings. China Quality Inspection Press: Beijing, China, 2020.
31. *JGJ 3-2010*; Technical Specification for Concrete Structures of Tall Building. China Architecture & Building Press: Beijing, China, 2010.
32. *GB 50011-2010*; Code for Seismic Design of Buildings. China Architecture & Building Press: Beijing, China, 2010.
33. *GB 55004-2021*; General Code for Composite Structures. China Architecture & Building Press: Beijing, China, 2021.
34. Cui, M.; Wang, C.; Chen, C.; Pan, Y.; Xiong, Y.; Ren, C. Seismic Resilience Assessment of Existing High-Rise Shear Wall Structure Based on Standard for Seismic Residence Assessment of Buildings. *Build. Sci.* **2023**, *39*, 47–53.
35. Ren, J.; Pan, P.; Wang, T.; Zhou, Y.; Wang, H.; Shan, M. Interpretation of GB/T 38591-2020 'Standard for Seismic Resilience Assessment of Buildings'. *J. Build. Struct.* **2021**, *42*, 48–56.
36. Zhao, L. Seismic Performance of Square Concrete-Filled Steel Tubular Assembly Columns Connected by Grout Anchors. Master's Thesis, Chongqing University, Chongqing, China, 2022.
37. Wang, H. Axial Compressive and Seismic Behavior of Spiral-Confined Ultra-High-Strength Concrete-Filled Square Steel Tube Columns. Master's Thesis, Huaqiao University, Quanzhou, China, 2020.
38. Zhang, J.; Li, Y.; Zhou, L.; Huang, Y. Experimental Research on Seismic Behavior of Concrete-Filled High Strength Cold-Formed Rectangular Steel Tubular Columns. *J. Guangxi Univ. (Nat. Sci.)* **2019**, *44*, 931–943.
39. Wang, M.; Yang, M. Experimental Study on Seismic Behavior of Square Concrete-Filled Steel Tube Column with End Ribs. *J. Hunan Univ. (Nat. Sci.)* **2017**, *44*, 31–37.
40. Zhang, J.; Lu, X.; Fan, Q.; Wu, S.; Wang, J. Experimental Study on Seismic Behavior of Recycled Aggregate Concrete Filled Square Steel Tube Columns. *Concrete* **2016**, *7*, 61–68.
41. Zhang, X.; Chen, Z.; Xue, J.; Su, Y. Experimental Study on Seismic Behavior of Recycled Aggregate Concrete Filled Square Steel Tube Columns. *J. Build. Struct.* **2014**, *35*, 45–56.
42. Nie, R.; Xu, P.; Yan, Y. Experimental Research and Finite Element Analysis on Seismic Behavior of Concrete-Filled Square Steel Tubular Columns. *J. Tongji Univ. (Nat. Sci.)* **2012**, *40*, 1596–1602.
43. Ma, K.; Liang, X.; Li, B. Aseismic Behavior of High Strength Concrete-Filled Rectangular Steel Tubular Columns with High Axial Load Ratio. *Eng. Mech.* **2010**, *27*, 155–162.
44. Li, L.; Li, N.; Chen, Z.; Jiang, X. Anti-seismic Test on Concrete-Filled Square Steel Tube Column. *J. Jilin Univ. (Eng. Technol.)* **2008**, *38*, 817–822.
45. Zhu, F.; Yu, Y.; Wang, Z.; Shi, G.; Liu, H. Experimental Study on Seismic Behavior of Monolithic Precast Double-Skin Composite Shear Wall. *J. Build. Struct.* **2023**, *44*, 146–156.
46. Sha, Z.; Xu, W.; Du, Y.; Si, X. Comparative Test on Seismic Performance of Double Steel Plate Composite Shear Wall with Multi Cavity Configuration. *J. Civ. Eng. Manag.* **2022**, *39*, 61–67.

47. Chen, L.; Xia, D.; Liu, W.; Zhang, X. Experimental Study on Seismic Behavior of Double Steel Plates and Concrete Composite Shear Wall. *Chin. Civ. Eng. J.* **2017**, *50*, 10–19.
48. Wu, J. Research on Seismic Behavior of High Strength Concrete Composite Shear Wall with Double Steel Plates. Master's Thesis, Guangzhou University, Guangzhou, China, 2012.